Glass-made adjustable integration mold for x-ray optics: experimental feasibility campaign

Losi, L., Civitani, M., Basso, S., Lavagna, M., Pareschi, G.

L. Losi, M. Civitani, S. Basso, M. Lavagna, G. Pareschi, "Glass-made adjustable integration mold for x-ray optics: experimental feasibility campaign," Proc. SPIE 11119, Optics for EUV, X-Ray, and Gamma-Ray Astronomy IX, 111190V (19 September 2019); doi: 10.1117/12.2529444

SPIE.

Event: SPIE Optical Engineering + Applications, 2019, San Diego, California, United States

GLASS-MADE ADJUSTABLE INTEGRATION MOLD FOR X-RAY OPTICS: EXPERIMENTAL FEASIBILITY CAMPAIGN

L. Losi[a,1], M. Civitani[b,2], S. Basso[b], M. Lavagna[a] and G. Pareschi[b]

[a]Politecnico di Milano, Aerospace Science and Technology Department, Via La Masa 34, 20156 Milan (MI), Italy;

[b]INAF Astronomical Observatory of Brera, Via E. Bianchi 46, I-23807 Merate (LC), Italy

ABSTRACT

Cold Slumping Glass Optics is a cost-effective technique to realize segmented X-ray optics. It is based on the replica approach: very thin flat glass foils are shaped to theoretical form by means of integration molds and fixed into stacks by means of ribs. As the theoretical shape of each of the layer depends on the radius of curvature inside the assembly, in principle different integration molds are needed to realize a stack. A worthwhile solution would be the usage of a single adjustable mold with an 'optical surface' to be shaped according to the position of the plate in the stack. The selection of the optical surface material and the bending strategy are the most relevant points. Glass would give major benefits in terms of thermal coupling with the glass foils, scratch resistance during operations and costs. On the other hand, given the reduced bending capability of the material coupled with its intrinsic fragility, experimental tests are necessary to assess the feasibility of the solution. In this paper we present the design and the implementation study as realized by the PoliMI-DAER. An experimental test campaign has been carried out beside the theoretical studies, to validate numerical models and obtain feedback from an early implementation. The test campaign is expounded along with the analysis of the results. A preliminary comparison with the numerical simulations is given.

Keywords: X-ray grazing-incidence telescopes, X-ray segmented mirrors, cold slumping, integration and alignment, reference mandrel, replication techniques

1. INTRODUCTION

Nowadays, Slumped Glass Optics (SGO) is a relatively new technology for the realization of X-ray optics[1,2,3,4] which has been already flight proven with the NuStar mission.[5] The process mainly relies on two phases: glass segments production with hot slumping and successive assembly into modules.

Within this context, INAF/OAB has developed an Integration Machine (IMA) to assemble Slumped Glass Optics mirror modules by means of the hot/cold slumping integration process; in these years the development is focusing on cold slumping, and optics with the technology have been proposed for the future X-ray telescope missions,[6] i.e. Force or AXION.[7] The Cold Slumping process starts directly from thin flat glass sheets and exploits Wolter-I counter form mandrels and reinforcing ribs for the realization of a full optic: The glass sheets are bonded with the ribs onto a supporting structure while at the same time they are wrapped on reference mandrels. The full optic is composed of an assembly of consecutive glasses in Wolter-I configuration, each one characterized by a different set of parameters. The advantages of this new approach are the low weight and low cost of the optics. In particular, avoiding hot slumping procedure, the realization costs and the production time are highly reduced. Furthermore, with cold slumping, micro-roughness of the glass foils is preserved.

Given that each pair (paraboloid + hyperboloid) of the several layers that compose a final optic assembly is characterized by different Wolter-I parameters, a complete set of reference mandrel pairs is needed to build a mirror module. Moreover, the mandrels shall be replaced and re-aligned for each different glass layer. A pair

Further author information:

[1]E-mail: luca.losi@polimi.it, Telephone: +39 02 2399 8024

[2]E-mail: marta.civitani@brera.inaf.it, Telephone: +39 039 5971028

Optics for EUV, X-Ray, and Gamma-Ray Astronomy IX, edited by Stephen L. O'Dell, Giovanni Pareschi, Proc. of SPIE Vol. 11119, 111190V · © 2019 SPIE · CCC code: 0277-786X/19/$21 · doi: 10.1117/12.2529444

of integration mandrels can be used for a subset of mirrors, exploiting the relative re-alignment of the molds pair to compensate for the taper angle between the parabolic and hyperbolic segments. This technique has been already successfully tested[8] but it is not a complete solution to problem due to the azimuthal aberration introduced. For these reasons, the most cost-efficient solution to the problem could be the exploitation of adjustable integration mandrels able to deform and mechanically adapt their geometry to cover all, or at least a subset, of the mirror module glass geometries. The feasibility study and assessment for the realization of such an adjustable integration mandrel is the main objective of the work hereafter presented. In this paper, an overview of the design and preliminary implementation study, as developed by PoliMI Department of Aerospace Science and Technology (DAER), is provided.
The current integration procedure is summarized in Section 2. The adjustable integration mold geometry and design, along with the numerical simulations, are briefly described in Section 3, the experimental test campaign carried out beside the theoretical studies is then expounded in Section 4, along with a brief comparison between experimental and numerical results. Finally, the conclusions are reported in Section 5.

2. INTEGRATION PROCEDURE

The cold slumping process currently adopted at INAF-OAB to build an X-ray module starts from the initial flat shape of the optic's glasses that has to be corrected to the final Wolter-I configuration.[8] Machine milled segmented molds (parabolic and hyperbolic in Wolter-I configuration) are exploited as reference mandrel to form the mirror plates via vacuum suction during the integration process. When forced onto the integration molds, the glass plates accurately replicate its shape. In this configuration, the first pair of glass foils are bonded to a stiff reference structure which will be later used for the integration. The subsequent mirror plates are bonded to the previously integrated ones in the stack by means of ribs, and so on. The procedure is schematically shown in Figure 1. Due to the initial difference in shape between the integration molds and the glass plates, spring-back effects are expected after the vacuum release of the latter. These effects are low at ribs location and increase with the distance of the latter. Accuracy of the integrated plates is therefore improved by optimizing the adopted ribs number and spacing. A detailed description is explained in references[9] and.[10]
The Integration MAchine, available at the INAF/OAB, allows the cold slumping integration process as well

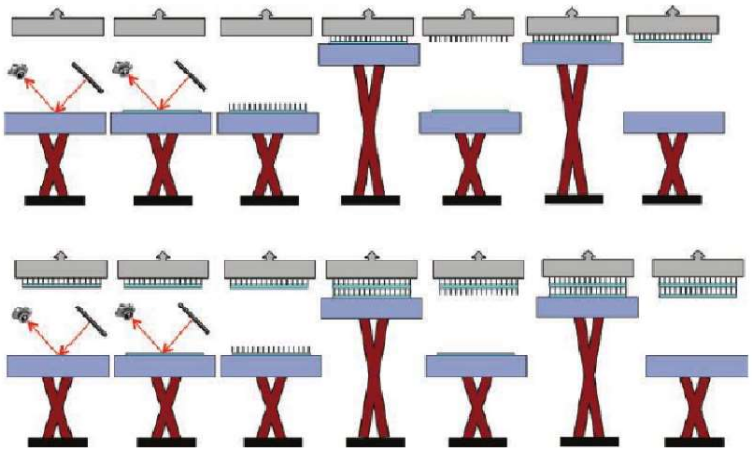

Figure 1: Mirror integration process flow at INAF-OAB.[8]

as the mutual plate alignment.[8] The relative alignment of the integration molds is carried out by means of picomotors acting on the hyperbolic mold in close loop with autocollimators. As each tandem of plates is bonded at a time with a very low shrinkage epoxy but long curing time, this active control avoids possible misalignment caused by thermal drifts.

3. CONCEPTUAL DESIGN

The realization of an adjustable mold able to cover the different glass geometries that constitute an X-ray mirror module implies that the key variables to work on are those that characterize the geometry of a hyperboloid or paraboloid surface: namely the radius of curvature, the conical angle and the longitudinal profile. The study case proposed in[8] is taken as reference. It is a medium-size X-ray module with focal length set to 8.4 m and radial size between 80 and 240 mm i.e. compatible with FORCE mission. The overall variation of the average azimuthal *sag* from the first mirror layer to the last one is of almost 50 mm. This is a too demanding target to be achieved through the deformations of the same adjustable surface. Thus, a simplified configuration, which takes into account only the external 20 layers of the mirror assembly, has been used. In this way, the target deformations are reduced to approximately 2.5 mm in azimuthal direction and maximum 0.05 mm in azimuthal top/bottom difference for a single sheet, with a range of 0.01 mm between the different plates. The differences in longitudinal profile are of the order of tens on nano-meters and therefore their effects on PSF are negligible. These values are considered as the working range requirements for the design.

3.1 Material trade-off

Material	**Density** [kg/m^3]	**Young modulus** [Gpa]	**Poisson ratio**	**Yield stress** [Mpa]	**Bend strength** [Mpa]	**CTE** [μm/m°C]
Borofloat33	2200	64	0.2	//	25	3.25
Titanium	4430	113.8	0.342	880	//	8.6

Table 1: Borofloat glass and Titanium mechanical properties.

Because of the high number of mechanical operations that will be carried out on the mandrel during integration, the mandrel's surface is exposed to scratches and damage that could affect the optical quality of the mirrors. Therefore, the mold surface must be very hard, scratch-resistant, and easy to clean. In addition, due to the mechanical loads applied/used to deform the mandrel into the required geometrical configurations, the material must also have good mechanical properties.
Since now, both aluminum and glass have been used to build a single integration mold at INAF/OAB premises. Aluminum, however, has not held up against scratches and cleaning operations. In addition, aluminum has a large CTE coefficient with respect to that of the mirror's glass. For these reasons, the aluminum solution has been discarded. On the other hand, the glass solution has instead shown good performance and is considered to be a good candidate material for the mold. In particular, the Borofloat33® glass by SHOTT is considered.[11] It has good mechanical properties, coupled with a CTE that matches with the glass adopted for the mirrors assembly. In addition, Borofloat33® is highly resistant to degradation by water, strong acids, alkalis, etc., making it an easy material to clean.
Among metals, Titanium matches well with the CTE of the assembly glasses, and has good mechanical resistance, high elastic modulus, resistance to corrosion and oxidation.[11] Although Titanium would require high forces to bend it into a desired shape, the high yielding stress, guarantees the achievement of relatively large deformations while remaining in the elastic field. On the other hand, compared with Borofloat33®, Titanium does not guarantee good interfacing with the optics, because of the high level of roughness of its surface, which could affect the surface properties of the assembled mirrors. Despite Titanium being still under investigation to be used for the realization of the integration mold, with different test undergoing, focus is hereafter posed to the glass solution only. Comparison of Borofloat33 and Titanimu mechanical properties are expounded in Table 1.

3.2 Numerical simulations

The main objectives of the numerical simulations performed are the assessment of the stress acting on the hypothetical mandrel body and the identification of the necessary loads to obtain the desired shape deformations. For the sake of simplicity, actuation of the paraboloid segment only is considered. The paraboloid glass geometry for each optic layer is the target function, while the actual configuration of the mandrel determines the initial conditions on which to apply an optimal set of loads to obtain the desired deformation.

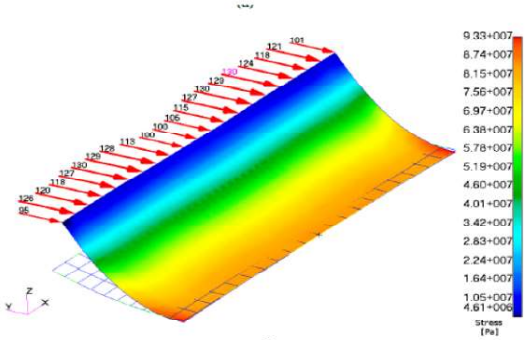

Figure 2: Load configuration identification with Nastran® local optimization. Maximum principal stress distribution is shown on the mandrel surface

As far as the actuation is concerned, a set of distributed loads can deform the mandrel. These may be applied either all over the underside of the mold surface or only on its edges. While the first solution may appear to offer the best precision and control of the system, the highly concentrated forces needed might introduce unacceptable local deformations on the mandrel surface. For this reason, the second solution has been investigated.
To meet the deformation range and sensibility requirements, focus must be placed on the control of the mandrel profile sagitta deformation along the azimuthal direction. This is the most sensitive parameter and requires major actuation along the lateral and vertical directions of the mandrel body. Deformations along the longitudinal direction, on the other hand, being very small from layer to layer and given that the already implemented IMA alignment control system is sufficient to compensate for small errors, have been disregarded.

A paraboloid plate of 250 mm × 250 mm × 4 mm accurately reproducing the first external mirror layer of the X-ray reference optics, modelled with plate elements, has been used for the analysis. Both local and global optimization methods have been implemented. First, a local optimization method has been adopted, which is a gradient based algorithm already present in Nastran®. Next, a wrapping tool which interfaces with Nastran® to perform global optimization exploiting particle swarm techniques (both Particle Swarm Optimization PSO and Multi Objective Particle Swarm Optimization have been adopted) has been developed with Matlab®. Two different thicknesses of the reference mold have been considered: 3 and 5 mm respectively, with some simulations performed considering also thickness itself as an optimization parameter. Half plate model has been exploited thanks to the geometry configuration symmetry, while constraints on the plate have been applied in a single point at the geometrical center. In such a way the overall reaction forces are null when load is applied and contribution of the constraint to stress distribution is null too. Detailed modelling of the mandrel support has

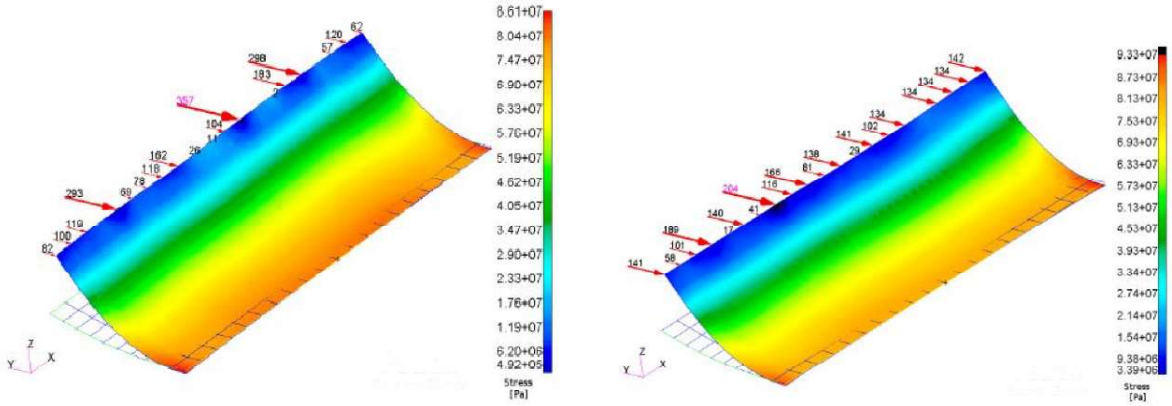

(a) PSO with 3mm Borofloat mandrel. (b) Experimental set-up overview during a test.

Figure 3: Load configuration identification with a) PSO and b)MOPSO on a 3mm Borofloat glass paraboloid plate.

not been considered at first and will be assessed in future development. Figure 2 shows the results obtained with a simulation run on a mandrel surface of 3 mm thickness. The high sensitivity demonstrated by the optimization algorithm w.r.t. small variations on initial conditions has suggested to move to the global optimization methods to search for a more reliable solution. Overall stresses are way above the bending stress limit for Borofloat®, at least theoretically as will be shown in later sections.
Figure 3 shows some of the results obtained with the global optimization methods, a 3 mm thick reference surface is considered. Figure 3a gives the load distribution and maximum principal stress obtained with the PSO; This approach has given some problems working on the objective function, which have been addressed with the MOPSO solution, shonw in Figure 3b. With the latter approach, an overall Root Mean Square Error (RMSE) between the obtained and target deformations from the starting mold configuration to the one which covers all the 20 mirror layers equal to 0.107 mm has been obtained. Despite not complete, these analysis allowed to gain sensibility with the finite element model and the problem itself. A preliminary set of loads has been obtained, at least in terms of order of magnitude, together with the expected stress distribution on the mandrel. A first basis of comparison for the experimental results on glass specimen has been therefore built.

4. EXPERIMENTAL TEST CAMPAIGN

Literature offers limited information on the mechanical properties of the Borofloat glass. Throughout this work, the maximum stress limit before failure for the numerical analysis is set to 25 MPa, equal to the one reported in[11] as bending strength. This value is quite low for the application here considered: from the results discussed in Section 3, the Borofloat® plate should be able to withstand stresses of the order of 90 MPa.
In order to obtain more certain information on the properties of this borosilicate glass, it has been decided to perform a series of experimental tests. To this aim, glass specimens have been produced with shape similar to the one of the reference paraboloid surface used for the numerical tests. The specimen are curved, rectangular plates of Borofloat33® with size of 150 mm × 50 mm and a radius of curvature of around 200 mm. In order to be consistent with the models adopted in the numerical simulations, samples of 3 mm and 5 mm thickness have been produced, for a total of 40 specimen. Example of two glasses ready to be tested are shown in Figure 4a for reference.

The samples have been procured flat. Then, the desired curved shape has been obtained with a dedicated

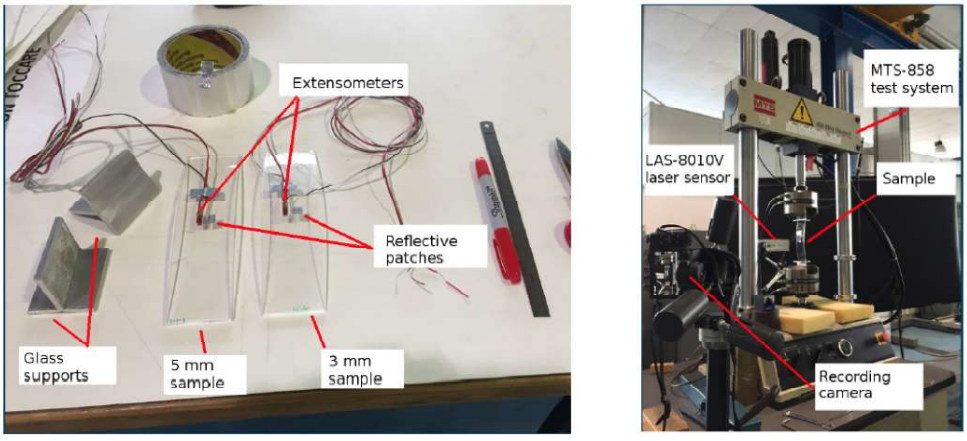

(a) (b)

Figure 4: Overview of the experimental set-up. a) Specimen preparation before test, b) running test.

thermal process at INAF/OAB. Annealing procedure has been applied to half of the specimen, with the aim of relieving eventual residual stresses originated during the cooling phase; residual stresses are in fact a potential major contributing factor in the fracture of fragile materials.
Before undertaking the tests campaign, photo-elastic measurements have been performed to highlight eventual

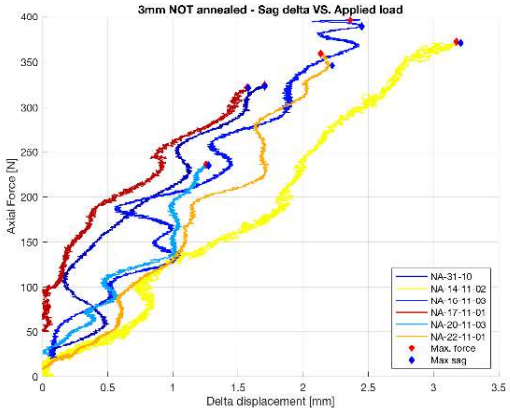

(a)

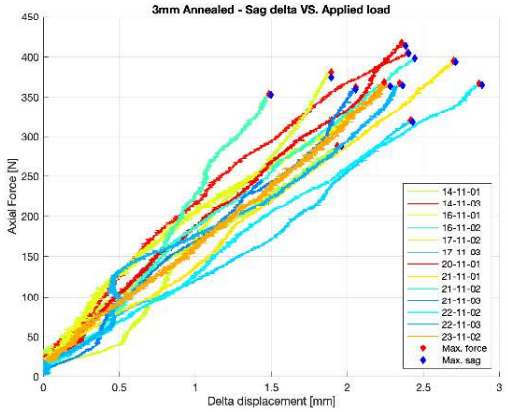

(b)

Figure 5: 3 mm glasses sagitta variation against applied force. a) Not annealed specimen, and b) Annealed specimen.

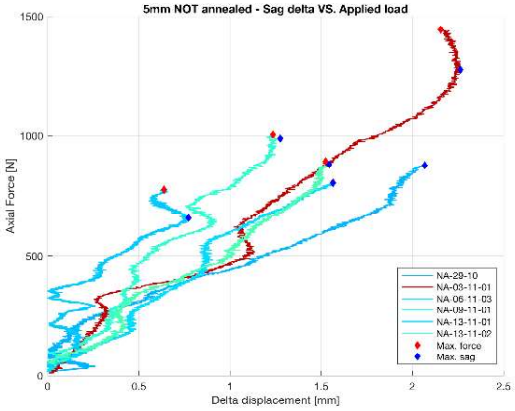

(a)

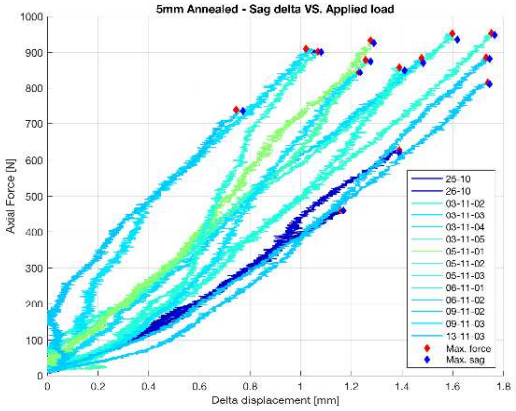

(b)

Figure 6: 5 mm glasses sagitta variation against applied force. a) Not annealed specimen, and b) Annealed specimen.

residual stresses still present in the Borofloat samples. These measurements allowed to have a better characterization of the specimen and consequently a better interpretation of the successive test results. Measurements have been obtained with two different polariscope instruments: a *030 Series Modular Reflection Polariscope* from the Vishay Measurements Group[12] and a *Strainoptics inc. Grazing Angle Surface Polarimeter* GASP.[13] Results from the test have shown very low values of residual stresses on the surface of the samples analyzed, in the order of 0.73 MPa. This result is inline with expectations, considering the long curing time used during the specimen realization, coupled with the low thermal gradient profile applied. Very low residual stresses could be expected on the surface of the samples even before the annealing procedure.

The experimental test campaign has been carried out at PoliMI-DAER facilities. Main objective was to retrieve the stress variation on the samples during the compression process and to measure the maximum middle section sagitta displacement that could be achieved on the plate. The test bench exploited is a *Material Testing System MTS-858*.[14] A dedicated support has been designed and realized to interface the edge of the glass specimen, where the load is applied, with the machine's clamps. The sagitta displacement arising from the glass specimen compression has been measured using a dedicated high precision laser sensor. Two electrical

extensometers (KYOWA kfg-3-350-C1[15]) for each specimen side have been mounted to measure the deformations occurring on both sides of the glass middle section. Finally, a data acquisition card with dedicated software has been used to collect and save the experiment results. The experimental value of the stress on the specimens have been retrieved after post-processing the data exploiting the curved beam theory.
The hereafter expounded test procedure has been adopted for all the specimen:

- Glass preparation with cleaning and strain-gage application (Figure 4a).
- Sample fixing on the MTS machine clamps. Position check.
- Calibration of all the measurement instruments.
- Test initialization with gradual compression applied until specimen rupture. MTS is displacement-controlled.
- Data gathering and storage.
- Data post-process and analysis.

The test configuration is depicted in Figure 4b: one of the 5 mm samples is mounted on the test bench, the laser sensor is pointing to the reflective patches, while the camera in the foreground was used to record the sample behavior during the test.

4.1 Results obtained

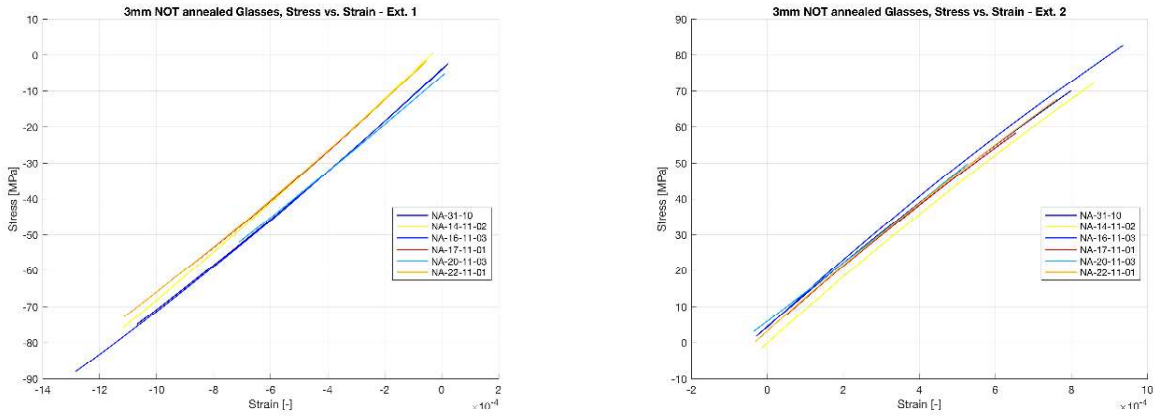

(a) (b)

Figure 7: 3 mm Not annealed glasses Stress-Strain curves. a) Gauge 1, under compression, and b) Gauge 2 under extension.

The overall test results in terms of sagitta displacement versus applied compression force are shown in Figure 5 and Figure 6, for the 3 mm and 5 mm glass specimen respectively. For each thickness considered, results are divided between annealed and not annealed glass. Curves exhibit a non expected non-linear behavior which is accentuated for the non-annealed specimens (see Figure 5a and 6a). Despite the apparently high deflections, those are of the order of 0.1 mm and completely not observable from the stress-strain curves of Figure 7,8 and Figure 9,10. Minor adjustment movement of the glass edges inside the machine supports could partially justify this behaviour. The usage of a rubber damper on the supports, after the first test conducted on non-annealed glass, further supports this hypothesis; more investigations are needed to verify this assumption.
Results in terms of stress-strain curves are here reported for both strain-gage under tension and compression: Figure 7 and Figure 8, a and b, for the 3 mm not-annealed and annealed glass specimens; Figure 9 and Figure 10, a and b, for the not annealed and annealed 5 mm specimens. All curves show small data dispersion and similar slope, a proof that the glass behave identically form an elastic point of view. It can be noticed that a slight

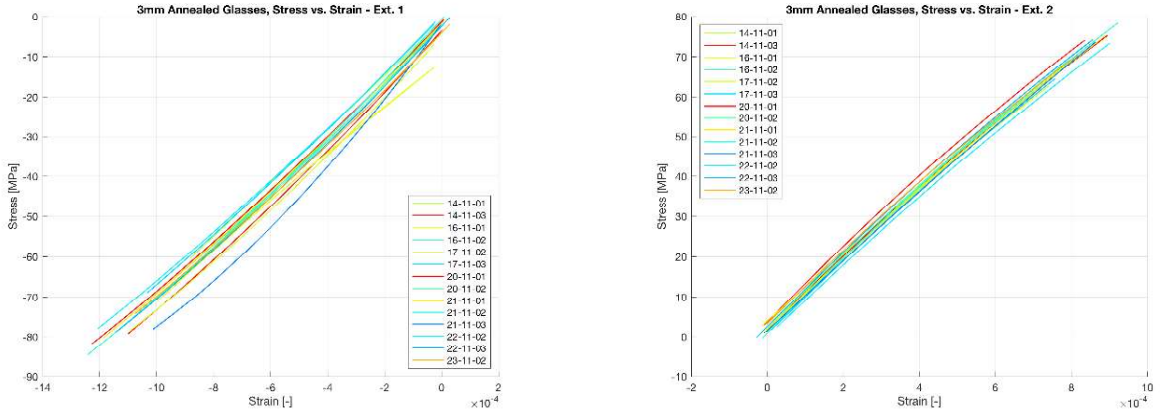

(a) (b)

Figure 8: 3 mm Annealed glasses Stress-Strain curves. a) Gauge 1, under compression, and b) Gauge 2 under extension.

variation in slope occurs comparing measurement results of the tests campaign performed on the two sides of the specimen (e.g. Figure 8a and 8b). This evidences a different behavior under compression and tension, as predicted by curved beam theory. In fact, considering the stress distribution in the middle cross-section of a generic curved beam, the theory predicts a non-linear behavior coupled with a neutral axis shift. This justifies the different results obtained for the two load conditions. Considering the failure points, stress at rupture is around 90 MPa for the thinner glass, while drops around 80 MPa for the thicker ones; all values are well above the theoretical one given in literature, corresponding to 25 MPa.

The results obtained have been further analyzed in function of the geometry of each specimen. Due to the

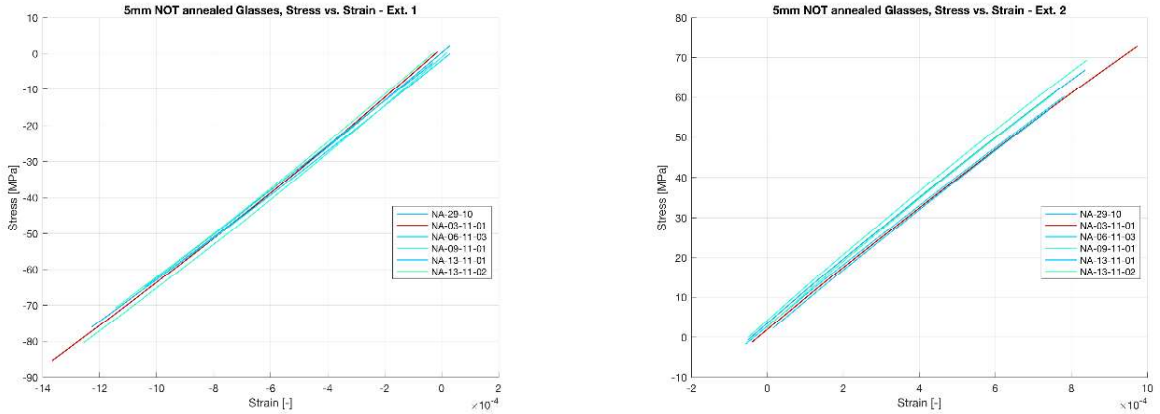

(a) (b)

Figure 9: 5 mm Not annealed glasses Stress-Strain curves. a) Gauge 1, under compression, and b) Gauge 2 under extension.

intrinsic characteristics of the realization process, the specimens present slightly different radius of curvature and longitudinal PtV. The longitudinal (or cross-section) Peak-to-Valley is defined as the maximum deviation of the specimen cross-section midline from the straight profile. Figure 11,12 and Figure 13,14 show the maximum force and sagitta delta at glass rupture against the different radius of curvature and cross-section PtV of each specimen tested. The azimuthal size of the samples is 150 mm. Curves are shown once again for the 3 mm and 5 mm thick glass. Despite the coherence with the curved beam theory, generally obtaining lower performance for

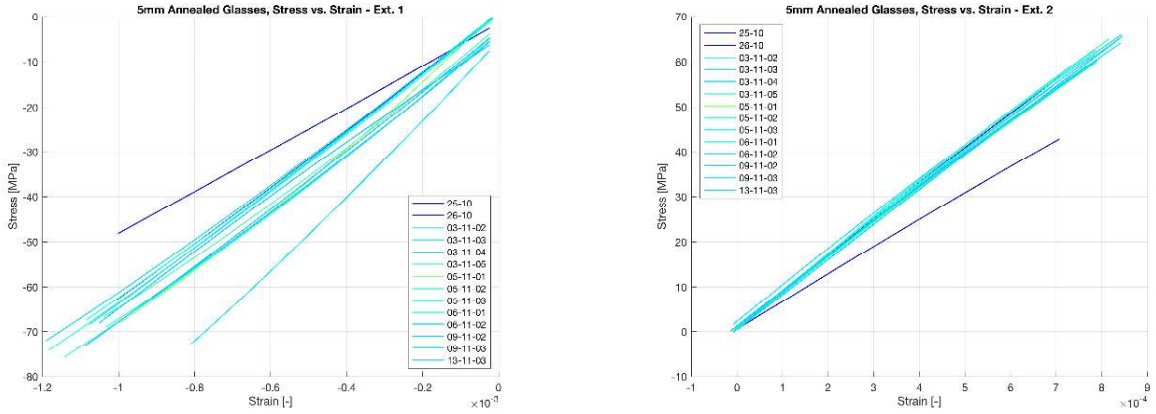

(a) (b)

Figure 10: 5 mm Annealed glasses Stress-Strain curves. a) Gauge 1, under compression, and b) Gauge 2 under extension.

samples with lower radius of curvature, a characteristic behavior for all the specimens is not evident from the plots, which instead highlight once again the highly unpredictable and randomic behavior of the brittle material. Table 2 and Table 3 give a summary of the main results obtained with the test campaign, in terms of average values and standard deviation, for the 3 mm and 5 mm thick specimen respectively.

3mm Annealed glass	**Mean**	**Std dev.**	
Maximum obtained sag displacement	2.195	0.423	[mm]
Maximum applied force	362.470	36.726	[N]
Maximum obtained stress in compressed section	-75.249	6.928	[MPa]
Maximum obtained stress in section under traction	69.882	6.423	[MPa]
Average Young modulus in section under compression	82.589	1.755	[GPa]
Average Young modulus in section under traction	66.342	3.577	[GPa]
3mm NOT Annealed glass	**Mean**	**Std dev.**	
Maximum obtained sag displacement	2.074	0.703	[mm]
Maximum applied force	334.684	56.499	[N]
Maximum obtained stress in compressed section	-70.540	12.665	[MPa]
Maximum obtained stress in section under traction	65.567	11.856	[MPa]
Average Young modulus in section under compression	82.455	1.549	[GPa]
Average Young modulus in section under traction	66.102	2.260	[GPa]

Table 2: 3 mm glass specimens, global experimental results.

4.2 Results comparison

The results obtained are comparable to those of the numerical simulations discussed in Section 3, suggesting that the model proposed is a good approximation of the real behavior of the plate. In particular, it can be noticed that the stress values obtained around breakage in the tests are similar to those obtained in the numerical simulations for a similar amount of deformation. All of that constitutes a good basis on which continue the work performing a correlation with the model adopted. With respect to these considerations, the Borofloat® glass can be considered a feasible solution for the realization of the adjustable mold, since it can cover at least a major part of the proposed target geometry configurations. Nevertheless, further tests and studies have to be made to increase confidence in the results obtained and to better characterize the Borofloat® behavior under the mechanical conditions described in this work.

5mm Annealed glass	**Mean**	**Std dev.**	
Maximum obtained sag displacement	1.360	0.295	[mm]
Maximum applied force	832.072	137.269	[N]
Maximum obtained stress in compressed section	-67.648	7.201	[MPa]
Maximum obtained stress in section under traction	60.144	6.148	[MPa]
Average Young modulus in section under compression	75.462	4.818	[GPa]
Average Young modulus in section under traction	62.349	7.282	[GPa]
5mm NOT Annealed glass	**Mean**	**Std dev.**	
Maximum obtained sag displacement	1.581	0.539	[mm]
Maximum applied force	967.200	246.589	[N]
Maximum obtained stress in compressed section	-72.273	7.681	[MPa]
Maximum obtained stress in section under traction	63.703	5.955	[MPa]
Average Young modulus in section under compression	74.123	2.367	[GPa]
Average Young modulus in section under traction	61.484	0.953	[GPa]

Table 3: 5 mm glass specimens, global experimental results.

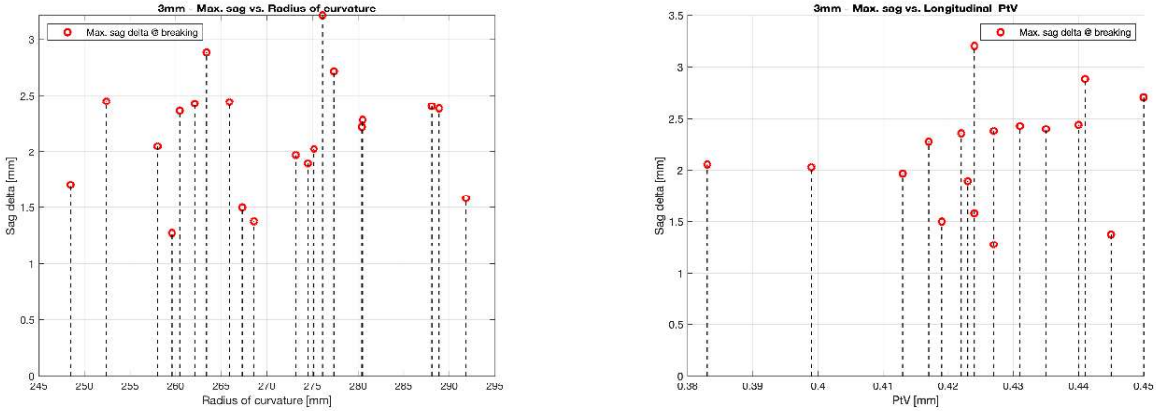

(a) (b)

Figure 11: 3 mm glasses maximum sagitta delta against a) Glass radius of curvature, and b) azimuthal PtV w.r.t. flat surface.

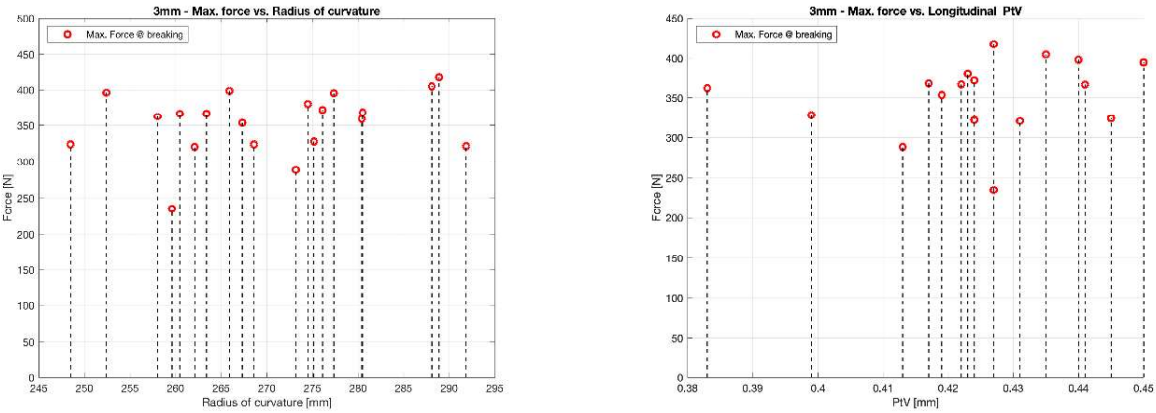

(a) (b)

Figure 12: 3 mm glasses maximum applied force against a) Glass radius of curvature, and b) azimuthal PtV w.r.t. flat surface.

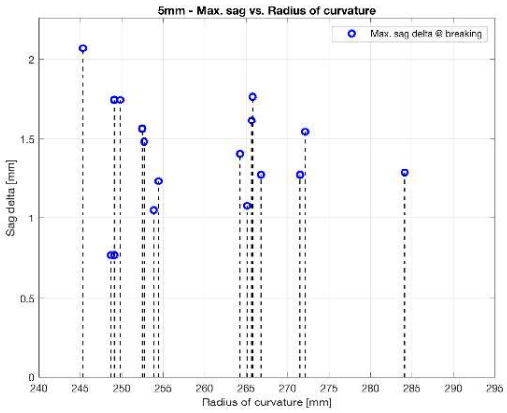

(a)

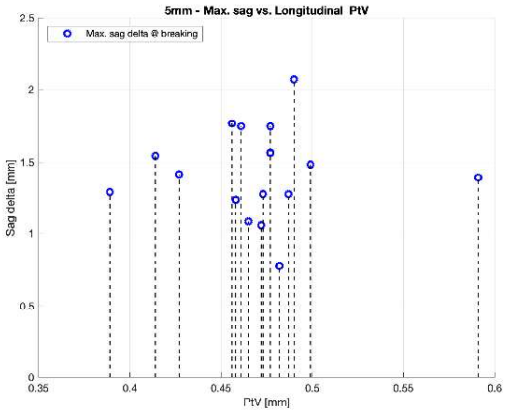

(b)

Figure 13: 5 mm glasses maximum sagitta delta against a) Glass radius of curvature, and b) azimuthal PtV w.r.t. flat surface.

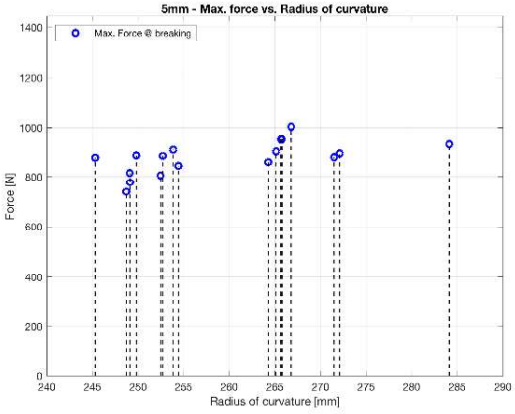

(a)

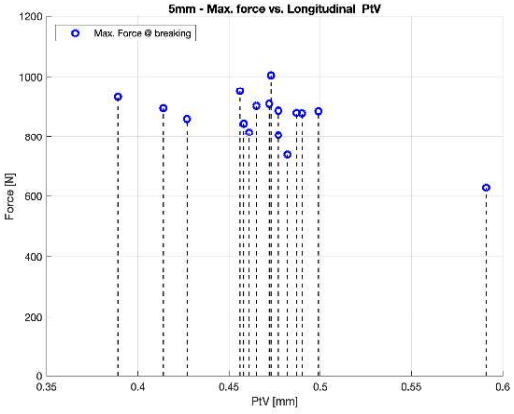

(b)

Figure 14: 5 mm glasses maximum applied force against a) Glass radius of curvature, and b) azimuthal PtV w.r.t. flat surface.

5. CONCLUSIONS

Modern X-ray optics are based on a nested system of hundreds of concentric mirrors. The fabrication of a high number of mirrors, each with different optical properties, is demanding in terms of production time and costs, as well as in terms of integration process complexity. This work studied the realization of an adjustable mold that can be shaped into different optical geometries to match the configuration of several X-ray reflective mirrors, an effective solution for the aforementioned criticalities. In particular, the best load configuration was searched, to obtain the required deformation with the desired accuracy. Two main optimization strategies have been adopted and integrated with the FEM analysis of the plate: a gradient based algorithm and a global optimization one based on Particle Swarm Optimization (PSO). For each approach, different simulation cases have been analyzed with different thickness of the mold, from 3 mm to 5 mm. The aim of the simulations was to impose a deformation on the mold such that, starting from the reference geometrical properties of a defined mirror, it would cover up to the shape of the wanted optical shell layer. Finally, preliminary experimental tests have been performed on Borofloat® glass specimen representative of a possible reference mandrel curvature; confirming that adjustable molds made of Borofloat33 can cover a wide range of plate pairs: With few sets of molds (5) it is possible to cover all the plate pairs forseen for FORCE w.r.t. the almost 100 needed without the adjustable molds. The obtained deformation of the plate resulted higher than expected, with maximum forces applied that are comparable to those obtained from the numerical simulations. Considering the Borofloat® optimal surface properties in addition to the mechanical performances obtained, this borosilicate glass could represent an innovative solution to be used for the adjustable mandrel realization.

ACKNOWLEDGMENTS

This project has been developed with the support of the Italian Space Agency (ASI). MSC Software Patran® and Nastran® have been used for the pre-process and post-process of all the structural analysis presented. A special thanks goes to Eng. Mauro Linari for the continuous support provided during the early stages of this work.

REFERENCES

[1] Zhang, W. W., Content, D., Lehan, J., Petre, R., Saha, T., Gubarev, M., Jones, W., O'Dell, S., and Reid, P., "Lightweight x-ray mirrors for the constellation-x mission," in [*Bulletin of the American Astronomical Society*], **37**, 1172 (2005).

[2] Ghigo, M., Basso, S., Canestrari, R., Conconi, P., Citterio, O., Civitani, M., Dell'Orto, E., Gallieni, D., Pareschi, G., Parodi, G., et al., "Hot slumping glass technology and integration process to manufacture a grazing incidence scaled prototype for the ixo telescope modules," in [*Optics for EUV, X-Ray, and Gamma-Ray Astronomy IV*], **7437**, 74370P, International Society for Optics and Photonics (2009).

[3] Chan, K.-W., Zhang, W., Saha, T., Robinson, D., Olsen, L., McClelland, R., Mazzarella, J., Lozipone, L., Lehan, J., Hong, M., et al., "An approach for alignment, mounting, and integration of ixo mirror segments," in [*Optics for EUV, X-Ray, and Gamma-Ray Astronomy IV*], **7437**, 74371D, International Society for Optics and Photonics (2009).

[4] Civitani, M., Basso, S., Bavdaz, M., Citterio, O., Conconi, P., Gallieni, D., Ghigo, M., Guldimann, B., Martelli, F., Pagano, G., et al., "Ixo x-ray mirrors based on slumped glass segments with reinforcing ribs: optical and mechanical design, image error budget, and optics unit integration process," in [*Space Telescopes and Instrumentation 2010: Ultraviolet to Gamma Ray*], **7732**, 773242, International Society for Optics and Photonics (2010).

[5] Craig, W. W., An, H., Blaedel, K. L., Christensen, F. E., Decker, T. A., Fabricant, A., Gum, J., Hailey, C. J., Hale, L., Jensen, C. B., et al., "Fabrication of the nustar flight optics," in [*Optics for EUV, X-Ray, and Gamma-Ray Astronomy V*], **8147**, 81470H, International Society for Optics and Photonics (2011).

[6] Basso, S., Civitani, M., and Pareschi, G., "Design of a medium size x-ray mirror module based on thin glass foils," in [*Space Telescopes and Instrumentation 2016: Ultraviolet to Gamma Ray*], **9905**, 990574, International Society for Optics and Photonics (2016).

[7] Jakobsen, A. C., Pivovaroff, M. J., and Christensen, F. E., "X-ray optics for axion helioscopes," in [*Optics for EUV, X-Ray, and Gamma-Ray Astronomy VI*], **8861**, 886113, International Society for Optics and Photonics (2013).

[8] Civitani, M., Basso, S., and Pareschi, G., "Adjustable integration molds for x-ray optics with cold shaping: requirements and conceptual design," in [*Space Telescopes and Instrumentation 2016: Ultraviolet to Gamma Ray*], **9905**, 990579, International Society for Optics and Photonics (2016).

[9] Parodi, G., Martelli, F., Basso, S., Citterio, O., Civitani, M., Conconi, P., Ghigo, M., Pareschi, G., and Zambra, A., "Design of the ixo optics based on thin glass plates connected by reinforcing ribs," in [*Optics for EUV, X-Ray, and Gamma-Ray Astronomy V*], **8147**, 81470Q, International Society for Optics and Photonics (2011).

[10] Civitani, M. M., Basso, S., Citterio, O., Conconi, P., Ghigo, M., Pareschi, G., Proserpio, L., Salmaso, B., Sironi, G., Spiga, D., et al., "Accurate integration of segmented x-ray optics using interfacing ribs," *Optical engineering* **52**(9), 091809 (2013).

[11] SCHOTT, "Borofloat® 33. the versatile floated borosilicate glass with an infinite number of applications," *Technical Glass Solutions GmbH* (2018).

[12] Vishay, M. I., "Photostress®instrumentation.full-fieldmeasurement systems for stress analysis and testing.," *Bulletin S-134-1* (1989).

[13] Inc., S., "Gasp instruments: For measuring surface stress in tempered, heat-strengthened, and annealed glass.," *Bulletin GSP-1218* (2018).

[14] Corporation, M. S., "Mts 810 and 858 material testing systems. versatile, multipurpose servohydraulic testing systems for static and dynamic tests," *MTS Systems Corporation, 14000 Technology Drive, Eden Prairie, MN, USA* (2018).

[15] KFG-KYOWA, "General-purpose foil strain gages kfg," *Kyowa Electronic Instruments Co., 3-5-1, Chofu-gaoka, Chofu, Tokyo 182-8520, Japan* (2018).